Si-C bonding in films prepared by heterofullerene deposition

P. Mélinon, X. Blase, P. Kéghélian, and A. Perez
Département de Physique des Matériaux, Université Claude Bernard-Lyon 1, F 69622 Villeurbanne, France

C. Ray, M. Pellarin, and M. Broyer
Laboratoire de Spectrométrie Ionique et Moléculaire, Université Claude Bernard-Lyon 1, F 69622 Villeurbanne, France

B. Champagnon
Laboratoire de Physico Chimie des Matériaux Luminescents UMR CNRS 5620, Université Claude Bernard-Lyon 1, F-69622 Villeurbanne cedex, France

(Received 13 September 2000; revised manuscript received 9 October 2001; published 12 March 2002)

We probed the electronic structure of mixed silicon-carbon Si_xC_{1-x} ($x=0.12$) films prepared from free silicon-doped fullerenes (heterofullerenes) deposited on silver thin film. The reactivity towards oxygen is also discussed. X-ray photoemission and Auger spectroscopies suggest that electron transfer from silicon to carbon atom is lower than in tetrahedral SiC compounds. Raman spectroscopy reveals a graphitization of the film associated with the formation of Si-C bonding under strong laser irradiation.

DOI: 10.1103/PhysRevB.65.125321 PACS number(s): 71.20.Nr, 71.23.−k, 72.80.Ng

I. INTRODUCTION

SiC crystalline phases have been extensively studied owing to their wide band gaps.[1] In all SiC polytypes, the lattice is formed by a periodic arrangement of sp^3 tetrahedral bonding silicon and carbon atoms with a perfect chemical ordering. Amorphous silicon carbides (a-Si_xC_{1-x}:H) have been also under research. These films are currently obtained by the radio-frequency (rf) glow-discharge[2] technique or by plasma-enhanced chemical-vapor deposition.[3] Such films have a large hydrogen content as observed in a-Si:H and are more or less described in terms of tetrahedral environment. Si_xC_{1-x} compounds with $x\neq 0.5$ are more complex and still debated since topological and compositional disorders introduce both the homonuclear and the heteronuclear bonds. The tendency of chemical ordering into an sp^3 network prevails in Si-rich films; conversely, the disorder increases in C-rich films.[4] In an earlier work, Mui and Smith[5] discussed the compositional disorder in terms of chemical ordering. Assuming a full sp^3 hybridization, these authors calculated the occurrence of both the homonuclear and the heteronuclear bonds in three models, namely, nonchemical ordering, chemical ordering with phase separation, and chemical ordering with homogeneous dispersion. More recently, Finocchi *et al.*[6] reported molecular-dynamics calculations performed in a SiC small cluster. They found a spread of the bonding type with a large homonuclear bond and a multiple hybridization. Conversely, Monte Carlo calculations[7] performed on amorphous stoichiometric SiC gives rise to an ordering trend. In a previous work, we studied Si_xC_{1-x} films with $x=0.5$ produced by low-energy cluster-beam deposition (LECBD).[8] Thin films were obtained by the deposition of preformed neutral clusters produced in a laser-vaporization source. The growth mechanism is more or less described in terms of ballistic deposition where clusters are randomly distributed on the surface without noticeable rearrangement. The films are then nanostructured with a partial chemical ordering. Three types of bonding were identified corresponding to Si-Si-, C-C-, and Si-C-rich regions, respectively. More recently, we have prepared thin films from the deposition of SiC heterofullerenes. Fullerene[9] structure can be looked upon as an alternative route with respect to sp^2- or sp^3-hybridized lattices. Fullerenelike structures are commonly reported for carbon, expected in silicon,[10–15] and currently observed in Si_xC_{1-x} (with $x\ll 0.5$) compounds.[16–20] Si_qC_{2n-q} heterofullerenes with $2n=32$–100 and $q<12$ are obtained by a substitutional doping of carbon with silicon. For example, Si_2C_{58} heterofullerene is derived from the C_{60} parent where two carbon atoms are replaced by silicon atoms. This paper deals with the electronic properties of Si_qC_{2n-q} heterofullerenes probed by Auger electron spectroscopy (AES), electron energy loss spectroscopy (EELS), x-ray photoelectron spectroscopy (XPS), and Raman spectroscopy. The electronic structure is compared to those observed in silicon and silicon carbide crystals.

II. EXPERIMENT

Silicon-carbon mixed clusters are formed in a standard laser-vaporization source. Further information is given in an earlier paper.[20] Briefly, a Nd:YAG (yttrium aluminum garnet) laser operating at 532 nm creates a plasma from a $Si_{\bar{x}}C_{1-\bar{x}}$ mixed target ($\bar{x}=0.12$). The mean stoichiometry $\bar{x}$ is defined as the percentage of silicon in the target. We use composite rods processed by binding silicon and graphite powders in various proportions. The quenching of the plasma by a pulsed high-pressure helium burst ensures the cluster growth in the chamber. The quenched plasma undergoes an adiabatic expansion through a nozzle giving a well-collimated beam formed by the mixing between clusters and helium. This geometry permits spectroscopic studies as well as the deposition of neutral free clusters far from the laser source. During the expansion, the cluster-growth process is controlled by a random stacking of Si and C atoms with $\bar{x}$ proportion. Owing to the statistic process (a Poissonian law), each cluster has a composition that differs from the initial $\bar{x}$ value. Neverthe-

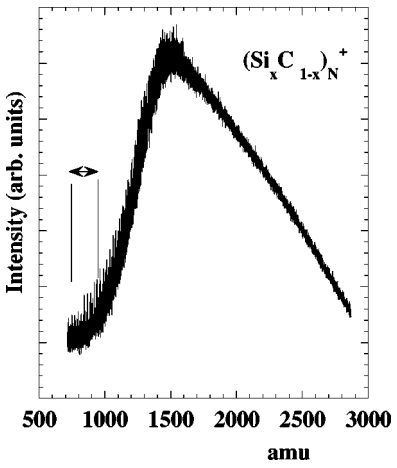

FIG. 1. Whole size distribution for $(Si_xC_{1-x})_N$ ionized clusters. The arrows indicate the window depicted in Fig. 3. The main number of atoms N is about ten.

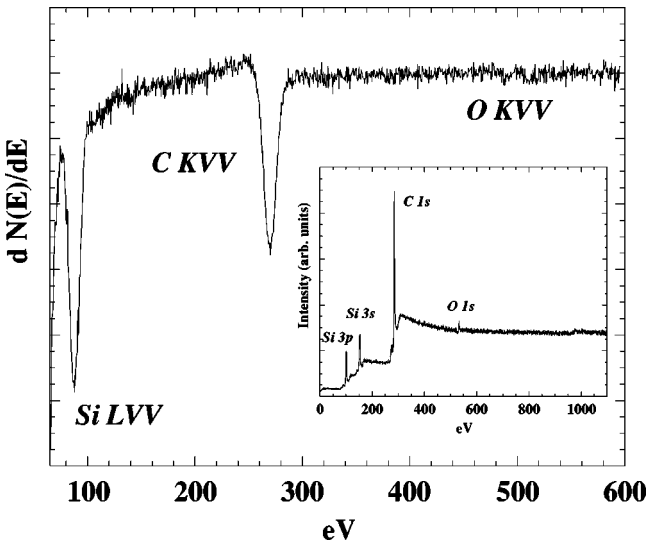

FIG. 2. Auger and XPS surveys showing the relative low concentration of oxygen. Despite the porous structure, the deposited film thickness is large enough to avoid the silver signal contribution. We do not observe the Ag $3d$ contribution at 368.3 eV.

less, it is easy to demonstrate that the stoichiometry of each individual free cluster Si_xC_{1-x} is nearly equal to $\bar{x}$ as far as the number of atoms inside the cluster becomes more than ten. In addition, the mean stoichiometry of the film deduced from XPS ($\bar{x}=0.12\pm0.03$) and Rutherford backscattering spectroscopy just coincides with the target one. We expect that the large spread $\Delta x=x-\bar{x}$ for the smallest sizes do not play a role for all the measurements mentioned below. Nevertheless, we must keep in mind that all the features are relevant to a ''mean'' effect and could not be related to the properties of a particular heterofullerene. Prior to deposition, the cluster-size distribution is measured in a high-resolution time-of-flight spectrometer equipped with a reflectron device. Neutral clusters are photoionized by a pulsed Ar:F excimer laser with 6.4 eV photon energy. Figure 1 displays the mass-size distribution of the Si_xC_{1-x} clusters.[21] If the neutral clusters have a low kinetic energy, the films grow following a simple ballistic model. They are nanostructured[22] with a high degree of porosity and can be compared to a ''nanosponge'' where the ''elemental block'' is the supported cluster itself. Contrary to the films partially crystallized, prepared by laser desorption,[23] the LECBD technique gives rise to amorphouslike films.[22] For all the experiments, the substrates are maintained at room temperature. Contrary to other methods, the nature and the temperature of the substrate are not a salient parameter for the film growth since the nucleation is totally achieved prior to deposition. Neutral clusters are deposited in an ultrahigh vacuum chamber ($<3\times10^{-8}$ Pa) and then transferred *in situ* in a microprobe of dual XPS/Auger CAMECA Nanoscan 100 type. XPS is performed using Al$K\alpha$ x ray (1486.6 eV) with a photoelectron energy resolution fixed at 1 eV. For AES and EELS, the primary electron energy is fixed at 2 keV (beam current 5 nA). Since the morphology of the film is nanogranular, the roughness plays an important role for Auger spectroscopy. We use an Auger microprobe operating at different magnifications (100 nm up to 10 μm spot diameter). We do not observe any significant effect in the position and the shape of the Auger peaks versus the magnification. This supposes that the charging effect is low. In both the XPS and AES, the energy of the ejected electron is measured with the same analyzer (cylindric mirror analyzer) operating at the same pass energy. This procedure ensures the best calibration in energy. We use XPS and AES together for determining the Auger parameter. This method raises the difference in charging effect, which results from incident x rays, versus electrons. Even though we cannot eliminate this dilemma, we checked on various metallic or insulator samples that the accuracy is better than 0.5 eV. Unfortunately, the silicon part in our films is too weak to observe a good signal-to-noise ratio on the *KLL* transition. Thus, we have analyzed the main transition corresponding to the *LVV* transition. During analysis, we have simultaneously probed the oxygen *KLL* transition (see Fig. 2). All the analyzed regions (100 nm up to 10 μm) do not reveal significant oxygen. Prior to deposition, the vacuum was down to 3×10^{-8} Pa. During the cluster deposition, the residual pressure increases up to 2×10^{-7} Pa mainly due to the residual buffer helium gas. The partial pressure of each component is measured by a gas analyzer (HIDEN analytical). The residual pressure due to the reactive components such as O_2, CO, H_2O, CO_2 was less than 10^{-8} Pa. Once the cluster film was done, the cluster beam is stopped and the residual vacuum becomes comparable to that observed prior deposition. The equivalent film thickness measured by a quartz balance monitor is about 50 nm and corresponds roughly to the stacking of 50–100 cluster monolayers. Owing to the porosity due to the nanogranular texture, the true thickness does not correspond to the equivalent thickness deduced from the quartz balance. The true thickness is measured from Rutherford backscattering spectroscopy and Talystep measurements and is increased by about a factor of 20–30 % compared to the equivalent thickness. For XPS/AES measurements, the substrate is a silicon wafer (111) coated by a thick silver film (200 nm) previously evaporated *in situ*. This thickness is large enough to prevent any contribution of the Si wafer during all the studies reported in this paper. Such a

procedure presents some advantages: a limitation of the charging effect, a good calibration[24] (the $Ag_{3d\,5/2}$ $=368.3$ eV is taken as reference), and a low oxygen contamination on the substrate (the residual atomic oxygen is less than 4%). Since the mean free path in the XPS/AES experiment is less than 2–5 nm, we expect that the signal arises from the top layer. In this paper, we report a high concentration of carbon (88%) (i.e., 12% of silicon) in the initial rod. This concentration is the best compromise between a significant silicon signal and a good yield for the heterofullerene production. Our sample is compared with other reference samples, namely a silicon wafer (111) labeled Si-2, a SiO_2 quartz, a C_{60} film obtained by the deposition of $(C_{60})_N$ clusters ($N>2$), and a wurtzite silicon carbide (labeled 2H-SiC). Prior to the experiments, Si-2 and 2H-SiC are chemically cleaned using methanol, water, and HF acid.[25] In addition, the core carbon lines are also compared with that of freshly cleaved highly oriented pyrolytic graphite (HOPG). Raman-spectrometry measurements are performed at room temperature using a DILOR *XY* confocal micro-Raman spectrometer. The heterofullerenes are deposited onto a 2-mm-thick cleaved lithium fluoride (LiF) substrate and then coated *in situ* with a 100-nm-thin silver film.[26] The thickness of the deposited Si_xC_{1-x} film is about 50 nm. Such sample geometry allows a Raman measurement through the highly transparent LiF substrate, the silver film deposited over the heterofullerene film acting as a protection barrier towards oxygen. Raman spectra are excited in the direction normal to the sample using the 514.5-nm line of an Ar^+ laser. The scattered light is also collected in the direction normal to the sample. The interface between the silver coating and the heterofullerene film is at the origin of a ''surface-enhanced Raman scattering'' (SERS) effect very convenient for analyzing our samples with the lowest possible laser fluence.[8] Nevertheless, we have observed that the Raman cross section differs for silicon and carbon atoms limiting the quantitative aspect of the measurements. This is emphasized for SERS spectroscopy.

III. RESULTS

A. Heterofullerenes: A brief overview

The fullerene structure is an alternative way to the conventional tetrahedral structure observed in bulk phase. In small covalent clusters, the surface atoms provide unpaired electrons that destabilize the network. As a result, a surface reconstruction occurs leading to a minimization of the so-called surface-to-volume ratio (i.e., close to the sphere) and/or a so-called ''rehybridization'' effect. This is well illustrated in the C_{60} fullerene with its spherical shape and its mean hybridization ($sp^{2.3}$) intermediate between graphite (sp^2) and diamond (sp^3). Another way is the saturation of the dangling bonds by hydrogen. This latter case corresponds to the a-Si_xC_{1-x}:H samples prepared by rf sputtering or chemical vapor deposition. In our case, our samples are hydrogen-free.[27] The signature of the heterofullerenes has been recognized by the careful analysis of the abundance-distribution and photofragmentation spectra. Figure 3 displays four narrow windows corresponding to the size distributions of Si_xC_{1-x} clusters deposited onto silver thin film with $\bar{x}=0$, $\bar{x}=0.12$, $\bar{x}=0.5$, and $\bar{x}=1$, respectively. We remember that for small clusters, the statistic combination leads to a spread of compositions ($\Delta x \neq 0$). Figure 3(a) ($\bar{x}=0$) shows pure-carbon clusters. The fullerene signature is partially recognizable by their parity: all the clusters have an even number of atoms. The selected window ranges between C_{62} and C_{78} (the whole size distribution is depicted in Fig. 1). We have depicted three different heterofullerenes ranging from $C_{62-q}Si_q$ to $C_{78-q}Si_q$ with $q=0$, 1, and 2, respectively. Upper values of q are possible but cannot be directly observed in the mass-abundance spectra owing to the mass overlapping (for $q=3$, $C_{57}Si_3$ coincides with C_{64}, for example). For comparison, Figs. 3(c) and 3(d) display Si_xC_{1-x} clusters with a mean stoichiometry $\bar{x}=0.5$ and pure silicon

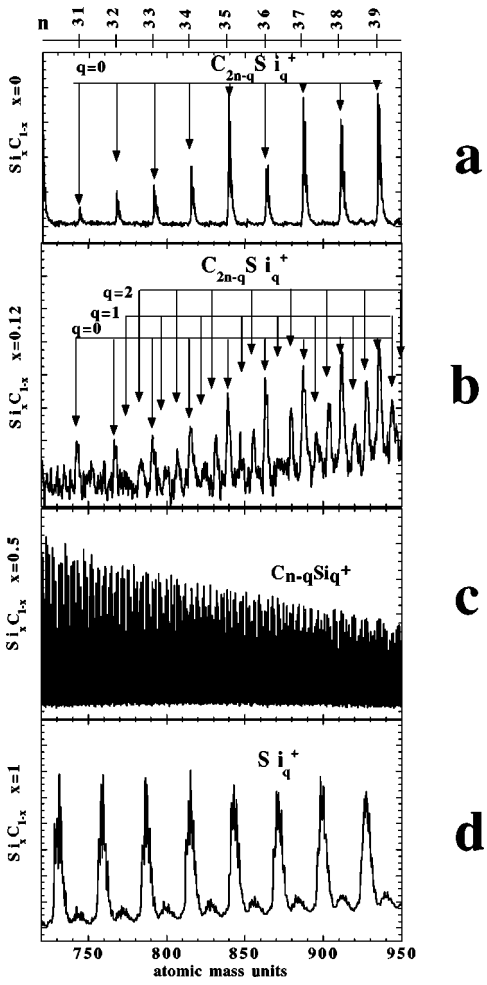

FIG. 3. Details of the mass-abundance spectra for different stoichiometries. (a) Distribution corresponding to silicon-free carbon clusters. (b) Displays Si_xC_{1-x} clusters with the mean stoichiometry $x=0.12$; the symbol $q=0$ corresponds to the pure carbon fullerenes, $q=1$ displays the fullerenes having one silicon atom, $q=2$ displays fullerenes having two silicon atoms, respectively. The periodicity is 8 amu. (c) Displays Si_xC_{1-x} clusters with the mean stoichiometry $x=0.5$, each peak corresponds to the statistic combination between the carbon and silicon isotopes; a fine analysis reveals a 4 amu (Ref. 8) periodicity according to a Poissonian law. (d) Distribution corresponding to carbon-free silicon clusters.

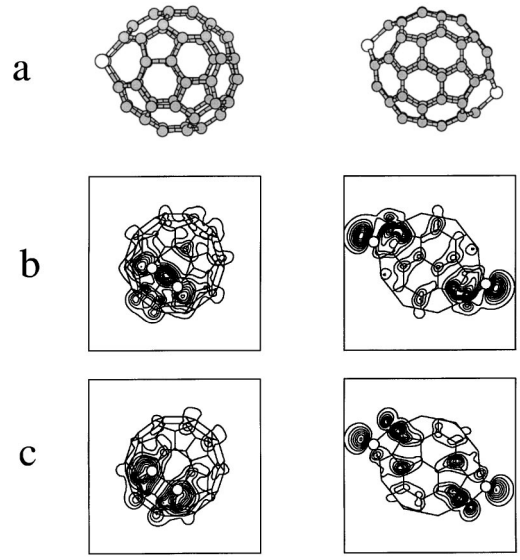

FIG. 4. (a) Symbolic ball-and-stick representation of meta-$C_{58}Si_2$ (right panel) and para-$C_{58}Si_2$ (left panel). Theoretical valence-charge density for HOMO (b) and LUMO (c) states in both $C_{58}Si_2$ isomers are also shown. We clearly see that lone orbitals are partially paired in meta-$C_{58}Si_2$. The details of the calculations are given in Ref. 19.

clusters ($\bar{x}=1$), respectively. For $\bar{x}=0.5$, all the combinations between silicon and carbon atoms (with their own isotopes) give rise to a great number of peaks leading to a 4 amu periodicity. For the heterofullerenes, the periodicity of the peaks is 8 amu [see Fig. 3(b)]. It has been established that such periodicity characterizes mixed Si-C clusters having even number of atoms as observed in pure fullerenes.[20] Since we deposit the whole size distribution, we are not able to characterize one selected heterofullerene. The observed features in our films arise from a collection of heterofullerenes with various sizes and compositions.

For instance, we illustrate the features of the heterofullerenes through $C_{58}Si_2$ and $C_{59}Si$. The details for the calculation are given in Ref. 19. Figure 4(a) shows the symbolic ball-and-stick representation of meta-$C_{58}Si_2$ (left panel) and para-$C_{58}Si_2$ (right panel). Figures 4(b) and 4(c) display the theoretical valence-charge density for the highest occupied molecular-orbital (HOMO) and lowest unoccupied molecular-orbital (LUMO) states, respectively. In meta-$C_{58}Si_2$, the creation of Si pairs involves a stabilizing energy with respect to a pure isolated dangling bond (see Fig. 4(b), left panel). The metaconfiguration is significantly more stable (0.76 eV) than the orthoconfiguration.[19] This ''rehybridization'' will be a signature of the heterofullerenes (with two silicon atoms or more) and differs significantly from the classical SiC phase. In addition, the dihedral angle between silicon and carbon atoms $\theta_{\pi\sigma}$ is close to that observed in an sp^3 lattice (109°,47). This occurs since the dihedral angles in the C_{60} parent ($\theta_{\pi\sigma}=102°$) lies between that in the sp^3 lattice and that observed in a threefold sp^2 ($\theta_{\pi\sigma}=90°$) lattice [see Fig. 4(a)]. This explains the protuberance formed by the silicon at the surface of the fullerene sphere. For $C_{59}Si$, energy-level calculation shows the appearance of two localized states (one donor and one acceptor) into the primitive band gap of the C_{60} parent fullerene.[19] This ensures that silicon provides a destabilization energy with respect on the pure C_{60} fullerene parent. All these features suggest that the silicon lone orbital offers all the characteristics of a dangling bond as observed in amorphous silicon. Although such heterofullerenes are stable enough to accommodate up to 12 silicon atoms, above this critical number, it has been suggested[20] that heterofullerenes undergo a phase transition towards more conventional SiC lattices derived from the crystalline form. Besides, the polarization of the Si-C bonds favors the chemical ordering in sp^3 SiC compounds while Si-Si pairing in heterofullerenes suggests a trend towards silicon ''clustering.''[19]

TABLE I. Core-level and electron-excited Auger lines for silicon (Si2p,LVV) and carbon (C 1s,KLL) observed in various samples. For the sample labeled II we indicate the two contributions after deconvolution.

Sample	Si 2p core-level line (eV)	Si LVV line (eV)	C 1s core-level line (eV)	C KLL line (eV)
Si-2	99.8	91.3		
2H-SiC	101.3	87.5	283.2	271.6
SiO	101.6			
SiO_2	103.2	78		
$Si_{0.12}C_{0.88}$ (I)	100.6	86.7	284.9	268.0
$Si_{0.12}C_{0.88}$ (II)	60% 100.6	84.7	284.9	267.5
	40% 101.5			
$Si_{0.12}C_{0.88}$ (III)	101.5	81.2	284.7	266.4
HOPG			284.8	268.8
C_{60} film			284.8	268.0

B. XPS measurements

The stoichiometry of the film is obtained by comparison of the yield ratio for Si 2p, C 1s, and O 1s core-level lines, respectively.[28] The atomic oxygen deduced from the ratio between Si 2p and O 1s after correction is less than 4%, not so far from the residual value observed in the silver thin film before deposition. In addition, a very weak oxygen component is observed in AES (Fig. 2). The experimental core levels are reported in Table I. The position of the O 1s line corresponds to that observed in CO or hydrocarbon molecules. The O 1s yield is low enough to neglect the oxygen role in the carbon line analysis. As regards the stoichiometry, we find $\bar{x}=0.12\pm0.03$ close to the initial concentration in the rod ($x=0.12$). Figure 5(a) shows the Si 2p core-level line observed in the Si_xC_{1-x} film. This line is located above Si 2p in Si-2 and beneath that in 2H-SiC. Though the charge transfer ΔE between silicon and one oxygen atom is similar to the transfer between silicon and carbon (SiC,$\Delta E=1.5$ eV; Si-O_2,$\Delta E=3.4$ eV), we expect that the presence of some oxygen pulls up the core-level line at higher energy. The Si 2p core-level line observed in our film could be slightly overestimated. Figure 5(b) displays the C 1s core-level line observed in the $Si_{0.12}C_{0.88}$ film. The line is beneath

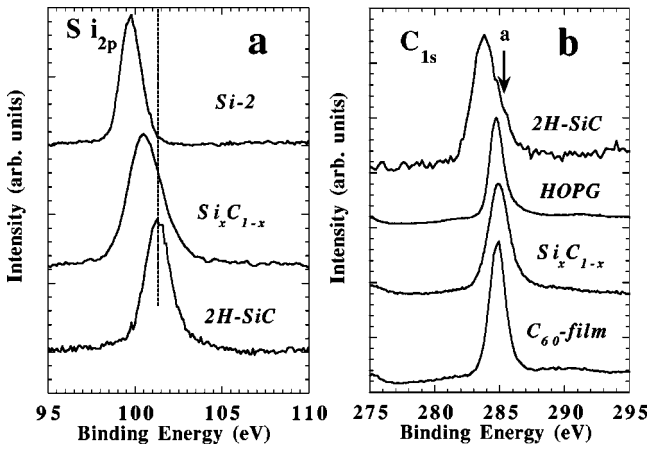

FIG. 5. (a) Si $2p$ core-level lines observed in Si-2, 2H-SiC, and $Si_{0.12}C_{0.88}$, respectively. (b) C $1s$ core-level lines observed in HOPG, 2H-SiC C_{60} film, and $Si_{0.12}C_{0.88}$, respectively. The arrow labeled *a* shows a shoulder attributed to the hydrocarbon contamination.

that in SiC 2H-4 and just coincides with the threefold hybridized carbon (HOPG) and C_{60} film. Besides, it has been found that the C $1s$ core-level line in the fourfold lattice (C $1s$ $=284$ eV in diamond phase) lies between graphite and silicon carbide.[29] The Si $2p$ and C $1s$ core-level shifts are also reported in *a*-SiC and[30,31] *a*-SiC:H in the carbon-rich region. This result is not adequate for a definitive conclusion. We need additional information derived from Auger spectra.

C. Auger spectroscopy

Figure 6(a) displays the silicon *LVV* lines observed in Si-2, SiC 2H-4, and $Si_{0.12}C_{0.88}$, respectively. It is well known that the Auger shift is enhanced compared to those observed by XPS. This occurs owing to the strong extra-atomic relaxation effects in the Auger process. The main band observed

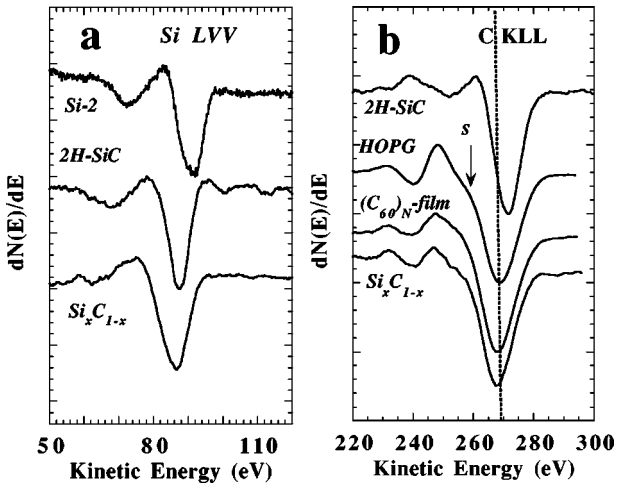

FIG. 6. (a) Derivative Si *LVV* Auger signal observed in Si-2, 2H-SiC, and $Si_{0.12}C_{0.88}$, respectively. (b) Derivative C *KLL* Auger signal in 2H-SiC, HOPG, C_{60} film, and $Si_{0.12}C_{0.88}$, respectively. The arrow labeled s shows the shoulder attributed to the π component.

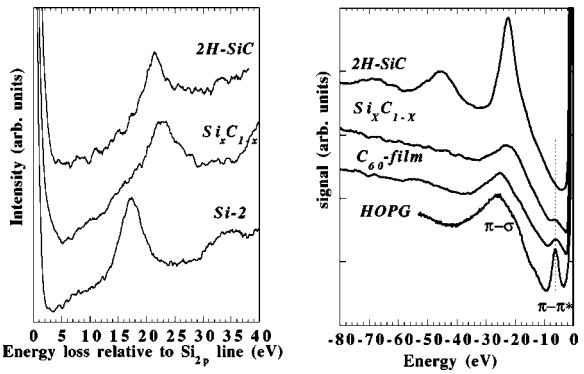

FIG. 7. Si $2p$ core-level lines and satellite peaks corresponding to the plasma losses observed in Si-2, 2H-SiC, and $Si_{0.12}C_{0.88}$, respectively. Plasma losses near the elastic electron-scattering signal observed in Si-2, 2H-SiC, and $Si_{0.12}C_{0.88}$, respectively, are also displayed.

in our sample ($E=86.7$ eV) is slightly shifted as compared to SiC 2H-4 ($E=87.5$ eV) and significantly differs from that observed in Si-2 ($E=91.3$ eV). This result is surprising since in a silicon compound, an increasing of the Si $2p$ core-level shift in XPS (binding energy) must be correlated to a decrease in energy (kinetic energy, KE) of the main Si *LVV* Auger band. In our experience, we clearly see that Si $2p$ in the cluster film is located beneath the position of Si $2p$ in 2H-SiC. If the chemical shift and the extra-atomic relaxation were equivalent in both materials, the Si *LVV* band in our cluster film should be located at higher KE with respect to 2H-SiC. The opposite case is observed that corroborates the assumption of a ''different'' Si-C environment in our cluster film. The Auger fine structure located at lower energy with respect to the main band is close to those observed in sp^3 hybridized silicon compounds. This is also consistent with a sp^3 silicon bonding as predicted in heterofullerenes. One has to remember that sp^2 hybridization is associated to a shoulder as observed in C $1s$ in graphite.[29] This shoulder is partially due to the contribution of the self-convolution of the π component in the electron density of states (DOS). Figure 6(b) displays the carbon *KLL* lines observed in 2H-SiC, HOPG, C_{60} film, and Si_xC_{1-x}, respectively. The *KLL* line in our cluster film presents some striking similarities with that in pure C_{60} film[32] even for the satellite peaks at low energy (especially the shoulder labeled *s* mentioned above). This shoulder, that indicates ''graphite,'' is less pronounced in both the Si_xC_{1-x} cluster film and the C_{60} film than in HOPG. This indicates that pure C_{60} fullerenes and heterofullerenes have a π-σ hybridization.

D. Electron energy loss spectroscopy/ ESCALOSS

Since plasma peaks are related to the free-electron density in the film, we probe mainly the coordinance and/or the type of bonding. Figure 7 displays plasma bands observed near the Si $2p$ region (electron spectroscopy for chemical analysis loss, ESCALOSS) and the plasma losses directly observed by electron-energy-loss spectroscopy. We take the origin of the energy ($E=0$ eV) from the Si $2p$ main core-level

line in order to eliminate the contribution of the core-level shift. Such a procedure gives us the plasma shift. In our Si_xC_{1-x} sample, the main plasma peak appears near 21 eV. This peak can be compared to those observed in 2H-SiC (22.4 eV), HOPG (27 eV), and C_{60} film (27 eV). The low value (21 eV) is mainly attributed to the low film density. This has been also reported in films formed by the deposition of free carbon clusters (i.e., $x=0$) with a mean cluster size of around $N=60$ atoms [see Fig. 2(a)].[33] The main band near 21 eV can be compared to the π-σ transition by reference to graphite. In addition, a weak but reliable band located at 6.4 eV in our Si_xC_{1-x} sample (only observed in the EELS spectrum) is assigned to π-π^* transition by reference with the graphite. Of course, this transition is not observed in 2H-SiC since all electrons are assigned to σ bonding.

IV. REACTIVITY

Finally, the type and the nature of the bonding can be readily probed through the reactivity between silicon and another atom, such as oxygen. For this purpose, we introduce oxygen into our apparatus (about 200 Torr). Figure 8 displays the evolution of the Si $2p$ [Fig. 8(a)] [C $1s$ Fig. 8(c)] lines as a function of the exposure time [oxygen-free (labeled I), 10^8 (i.e., 100 s) (labeled II) and 10^{12} (i.e., 15 days) (labeled III)] ($1\text{L}=10^{-6}$ Torr s). Roughly speaking, Si $2p$ binding energy increases with the exposure time. The shift is correlated with the increase in the O1s line yield. These effects are related to the silicon oxidation under oxygen exposure. We notice that the final position of the Si $2p$ line remains unchanged after 10^{12} L. The core-level shift (referred to pure silicon Si-2) in SiO_2($\Delta E=3.4$ eV) appears roughly at twice that in the sample labeled III ($\Delta E=1.7$ eV). Our value (sample III) is close to that measured in the SiO compound (Aldrich Company). All the observed lines are summarized in Table I. Contrary to silicon, the carbon line does not change significantly under oxygen exposure [see Table I and Fig. 8(c)]. A careful analysis shows that Si $2p$ core-level lines can be decomposed with two main lines located at 100.6 eV and 101.5 eV, respectively (Fig. 9). Prior to oxidation (sample I), the Si $2p$ line is well fitted by a line at 100.6 eV corresponding to our experimental data for Si-C bonding in the cluster film [Fig. 9(a)]. A careful analysis reveals two shoulders located at 99 eV and 103 eV, respectively. These satellite lines could be assigned to weak components corresponding to Si-Si (99.8 eV) and Si-O bonding in SiO_2 (103.4 eV). The Si-O bonding will be assigned to the native oxidation in the film as observed in the XPS survey (see Fig. 2). This native oxidation is located at the surface of the cluster film and partially disappears after ion etching in the dual XPS/AES apparatus. The sample labeled III [Fig. 9(c)] presents a shape asymmetry with a large shoulder at low-energy (99–100 eV). The spectrum can be modeled with one line located at 101.5 eV and a weak contribution in the region of 99–100 eV corresponding to Si-Si and/or Si-C bonding. Since the Si $2p$ spectrum remains unchanged with oxygen exposure, we believe that all the dangling bonds are satisfied with a Si-O bonding. It is interesting to note that the Si-O bonding is close to that in our SiO bulk sample rather than that observed in SiO_2. The sample labeled II [Fig. 9(b)] displays an intermediate case and could be decomposed with both the main lines observed in the samples I and III, respectively. In addition, two shoulders corresponding to Si-Si and Si-O bonding in SiO_2 are also observed. A plausible interpretation is the following one: since the clusters are not built from tetrahedral bricks, it is not possible to build up a $Si-O_4$ cell as observed in SiO_2. This effect has been also observed in pure silicon clusters.[26] The oxidation state corresponding to the label III is different from that observed by Ibrahim *et al.*[34] These authors studied the photo-oxidation of a-Si:C:H samples and found that interstitial oxygen did not appear bonded to silicon. Since our samples are hydrogen-

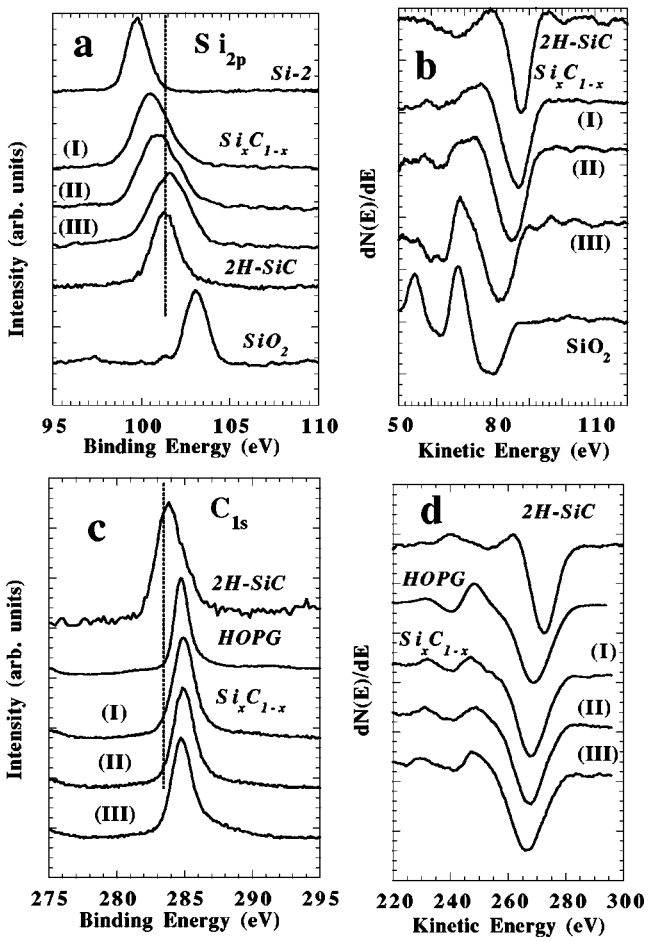

FIG. 8. (a) Displays the Si $2p$ core-level lines in our cluster film after oxygen exposure in I (free sample), II (i.e., 100 s), and III (i.e., 15 days). For comparison, we have displayed other reference samples, namely, Si-2, 2H-SiC, and SiO_2. (b) displays the Si LVV derivative Auger lines in our cluster films after oxygen exposure in I (free sample), II (i.e., 100 s), and III (i.e., 15 days). We have also displayed other reference samples, namely, Si-2, 2H-SiC, and SiO_2. (c) displays the C $1s$ core-level lines in our cluster film after oxygen exposure in I (free sample), II (i.e., 100 s), and III (i.e., 15 days). We have also displayed other reference samples, namely, 2H-SiC and HOPG. (d) displays the C KLL derivative Auger lines in our cluster film after oxygen exposure in I (free sample), II (i.e., 100 s), and III (i.e., 15 days). We have also displayed 2H-SiC and HOPG lines.

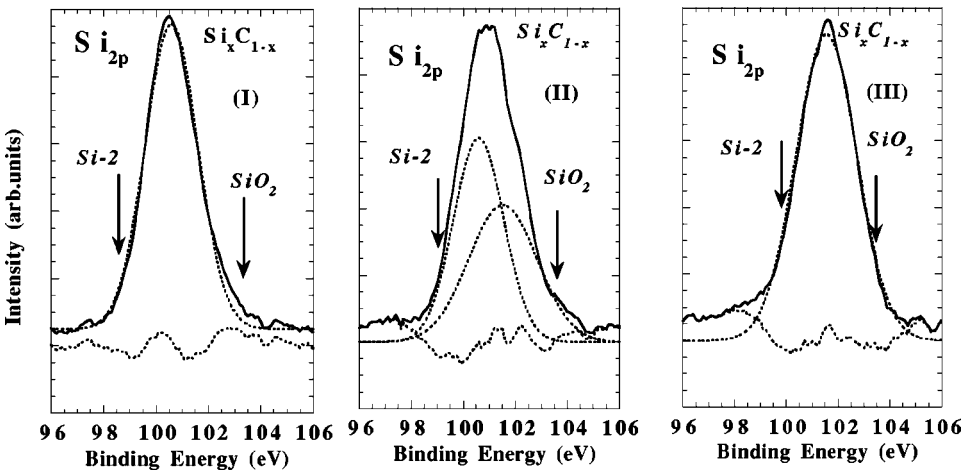

FIG. 9. Si $2p$ core-level lines at high resolution for $Si_{0.12}C_{0.88}$ labeled I, II, and III, respectively. The deconvolution of the spectra is shown with the residual signal (dashed lines).

free, the dangling bonds can be satisfied by oxygen bridging. The oxidation can be also observed in the Si *LVV* Auger spectra [Fig. 8(b)] since the extra-atomic relaxation energies between silicon and oxygen are significantly enhanced with respect to carbon. Prior to oxidation, the Si *LVV* Auger spectrum present some similarities with those in 2H-SiC [Fig. 8(b)] except the position of the main line (86.7 eV and 87.5 eV for Si_xC_{1-x}-cluster film and 2H-SiC, respectively). After oxygen exposure, the behavior of the Auger peak also changes drastically. Finally, the Auger features are close to those observed in the SiO_2 sample. Nevertheless, the main line observed in the cluster film after oxidation (sample III) is located at higher energy (81.2 eV) than that in the SiO_2 sample (78 eV). This result suggests that the oxidation is not complete ($Si\text{-}O_x, x<2$), in agreement with the XPS results. Figure 8(d) displays the C *KLL* line as a function of the time of exposure. We see that the Auger spectra remain similar, in agreement with the XPS data.

V. RAMAN SCATTERING SPECTROMETRY STUDIES

SiC bonding is often probed by Raman spectroscopy since vibrational modes and electronic structure are strongly correlated together. At low laser fluence ($P<1$ mW), no noticeable signal is observed in the cluster film Raman spectrum near the 500–1000 cm^{-1} region corresponding to the phonon DOS for SiC compounds. However, the Raman signal appears clearly (Fig. 10) by increasing the laser power up to 10 mW (the laser spot diameter on the sample is about 2–4 μm). This signal is attributed to the phototransformation of the clusters under laser irradiation[35] leading to a darkening of the irradiated area. The spectrum reported in Fig. 10 corresponds to a steady state (at 10 mW), where the spectrum remains stable under irradiation. After irreversible transformation, three main regions are identified on the spectrum. The region at high energy can be associated to a ''graphitization'' effect. The amorphous carbon phase formed in this case is responsible of the two bands[36] labeled *G* (near 1580 cm^{-1}) and *D* (disorder) near 1300 cm^{-1}. We also observe some bands at 766–815 and 965 cm^{-1} that characterize Si-C vibrational modes. Such bonds appear under laser irradiation and suggest that heterofullerenes are metastable. This is not surprising since pure carbon fullerenes (C_{60}, C_{70}) are also affected and polymerize under laser irradiation. In our case, the polymerization process can be strongly favored by silicon atoms with their lone orbitals. Two peaks labeled *a* and *b* in Fig. 10 are not assigned. This suggests the reminiscence of the Si-C vibrational modes in the surviving heterofullerenes prior to phototransformation. Moreover, a broadband located down to 450 cm^{-1} is the signature of Si-O-Si vibrational mode in SiO_x compounds ($0<x<2$) and/or in Si clusters. The presence of a Si clustering is surprising and is not reported from XPS and AES measurements. This suggests that the phototransformation could promote a clustering effect (XPS spectra were recorded without phototransformation). Moreover, we keep in mind that SERS spectroscopy strongly enhances the Si-Si contribution with respect to C-C and/or Si-C ones. At last, 766–815 cm^{-1} and 965 cm^{-1} peaks can be compared with the Raman allowed peaks[37] in the 2H-SiC crystal (see Fig. 10). The correlation between these modes and those observed in our sample is outlined. The sharpness of the bands after phototransformation supports the idea of a well-ordered SiC region in our cluster

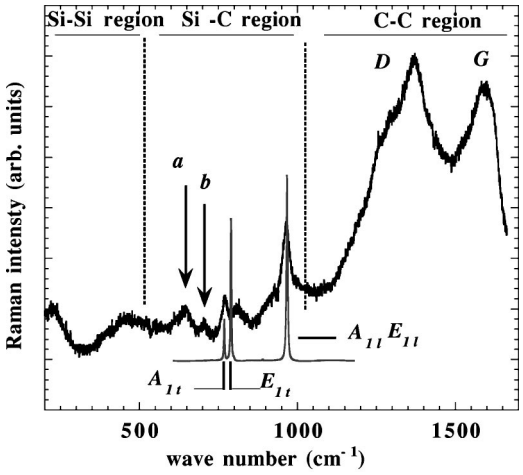

FIG. 10. Raman spectrum of the cluster film after laser irradiation. The 2H-SiC allowed lines and their symmetries are also reported for comparison. *a* and *b* arrows show unassigned bands. At the onset of the irradiation, no significant signal is observed on the cluster film.

films. These bands are largely independent of the polarization configuration as observed[38] in porous SiC.

VI. DISCUSSION

In summary, the hypothesis of a carbon tetrahedral structure is not consistent with Auger *KLL* carbon features and plasma losses. Nevertheless, the charge transfer shows that carbon atoms surround silicon. Since the observed charge transfer is less effective than in SiC bulk, we expect that silicon is weakly bound in heterofullerenes. This assumption will be discussed now. The striking differences between our sample and 2H-SiC are the following: (i) Si $2p$ in our sample lies between those observed in Si-2 and 2H-SiC, respectively. (ii) The Auger Si *LVV* line appears at lower energy than that observed in 2H-SiC. (iii) The fine structure is close to those observed in sp^3 silicon compounds. (iv) Plasma losses appear at lower energy with respect to 2H-SiC. Features (i) and (ii) are the more intriguing. In most of the silicon compounds, the core-level shifts ΔE_{chem} deduced from XPS are well correlated to those observed in Auger transitions. We remember that the chemical core-level shift ΔE_{chem} is usually obtained after summing two terms: the shift of the core level of a solid-state atom as compared to a free atom ΔE_{ini} and the polarization ΔE_{fin} due to the core-hole screening effect after relaxation. ΔE_{ini} can be estimated in tetrahedrally bonded materials characterized by an iono-covalent bonding.[39] However, it is difficult to calculate such values in our cluster films. Nevertheless, using the dielectric-model picture, we can estimate[40] the extra-atomic relaxation energy ΔE_{fin},

$$\Delta E_{fin} = (1 - 1/\epsilon_0)\frac{e^2}{2d_{eff}}, \tag{1}$$

where d_{eff} is a parameter that depends on the bulk plasma frequency ω_p and the Thomas-Fermi wave vector of valence electrons q_{TF}, and ϵ_0 is the static dielectric constant. Assuming that d_{eff} varies slowly, one gets a value for the variation of the extra-atomic relaxation energy ΔE_{fin},

$$\delta E_{fin} = \Delta E_{fin(\mathrm{SiC})} - \Delta E_{fin(clust)}. \tag{2}$$

This formula holds as long as dynamical effects (when the polarization of the electron cloud will not be complete) in the mechanism of relaxation can be neglected. For example, it has been found that dispersion minimizes the part of the relaxation energy in the total core-level shift for SiO_2 compound.[41,42] Since the silicon is surrounded by carbon atoms, the relaxation will be correlated to the relaxation energy of the carbon lattice. We take the value for the fullerene[43] ($\epsilon_{0(\mathrm{C}_{60})} = 4.3$) rather than the graphite ($\epsilon_{0(HOPG)} = 12$) or diamond phase[44] ($\epsilon_{0(diamond)} = 5.7$). Besides, $\epsilon_0 = 4.3$ ranges inside the values frequently observed in amorphous carbon films with the same plasma frequencies. The shift between 2H-SiC ($\epsilon_{0(\mathrm{SiC})} = 6.7$) and the film becomes[44]

$$\delta E_{fin} = -(1/\epsilon_{0(\mathrm{SiC})} - 1/\epsilon_{0(\mathrm{C}_{60})})\frac{e^2}{2d_{eff}}, \tag{3}$$

$$\delta E_{fin} = 0.04\frac{e^2}{d_{eff}}. \tag{4}$$

This calculation holds for silicon atom with $d_{eff} = 0.74$ Å, $\delta E_{fin} = 0.6$ eV. It indicates that the Si $2p$ line in our film would lie at 0.6 eV above that in 2H-SiC assuming the same type of bonding (i.e., the same charge transfer). Since the Si $2p$ line in our cluster film is located beneath that in 2H-SiC, the bonding is then different. The contribution to the initial state is more difficult to estimate. Taking our experimental data and Eq. (4) together,

$$\delta E_{ini} = E_{\mathrm{SiC}(2p)} - E_{clust(2p)} + \delta E_{fin} = 1.3 \text{ eV}. \tag{5}$$

Even though this value is overestimated, such an equation indicates a large decrease of the chemical bonding in our film with respect on the bulk 2H-SiC. E_{ini} increases as long as the ionicity (i.e., the electron transfer) increases. This is emphasized in silicon since the ionization of a free Si atom promotes a 9.4-eV shift of the $2p$ level to deeper energy. A small charge transfer in the cluster film can be related to the lone orbitals for silicon atoms inside the heterofullerenes. It explains the larger Auger shift. As pointed out in the literature, the Auger parameter[45,46] (AP) *A* is a common way for determining the change in the extra-atomic relaxation. In the sudden approximation, the chemical shift in the Auger parameter is equivalent to twice the difference in dynamic extra-atomic relaxation energies of an atom in different environments. For silicon, one gets

$$A_{(clust)} = E_{clust(LVV)} - E_{clust(2p)} = 2\Delta E_{fin(clust)}, \tag{6}$$

$$A_{(\mathrm{SiC})} = E_{\mathrm{SiC}(LVV)} - E_{\mathrm{SiC}(2p)} = 2\Delta E_{fin(\mathrm{SiC})}. \tag{7}$$

One also defines

$$\delta A_{(\mathrm{SiC}\text{-}clust)} = A_{(\mathrm{SiC})} - A_{(clust)} = 2\,\delta E_{fin}. \tag{8}$$

(The first bracket on the left-hand side of the equation is relevant to the Auger transition and the second on the right-hand side to the XPS core level.) Such a procedure improves the accuracy of the difference determination and reduces the systematic errors in the *A* determination. The *A* gives accurate[46] E_{fin} from the analysis of the both Si $2p$ and *KLL* transitions. Unfortunately, the too weak *KLL* signal-to-noise ratio discards its determination. However, we can estimate an Auger parameter by analyzing the *LVV* transition. We assume that the *A* shift determined from the *LVV* transition is proportional to that defined from *KLL*. Table II reports the measured *A* shifts compared to other reference states. From Eq. (8) $\delta A_{\mathrm{SiC}\text{-}clust} = 1.5$ eV, which is consistent with the prediction given by Eq. (4). Although, the Auger process emphasizes the role of the screening (there are two holes) with respect to the photoemission (with one hole), the total level shift is higher in the Auger spectrum.

Such a procedure can be also extended to the carbon lines,

$$A_{(clust)} = E_{clust(KLL)} - E_{clust(1s)}, \tag{9}$$

$$A_{(HOPG)} = E_{HOPG(KLL)} - E_{HOPG(1s)}, \tag{10}$$

TABLE II. Auger parameters defined for each sample.

Sample	$A(\mathrm{Si}) = \mathrm{Si}\ 2p + LVV$	$A(\mathrm{Si}) = A(\text{Si-2})$	$A(\mathrm{C})$
Si-2	191.1	0	
2H-SiC	188.8	2.3	554.8
$Si_{0.12}C_{0.88}$ (I)	187.3	3.8	552.9
$Si_{0.12}C_{0.88}$ (II)	185.7	5.4	552.9
$Si_{0.12}C_{0.88}$ (III)	182.7	8.4	551.1
SiO_2	181.2	10	
HOPG			553.6
C_{60} film			552.8

$$A_{(\mathrm{SiC})} = E_{\mathrm{SiC}(KLL)} - E_{\mathrm{SiC}(1s)}. \tag{11}$$

For carbon, we take HOPG as reference besides the difficulty to measure accurately both the C 1*s* and the *KLL* transitions in the carbon-diamond phase. One gets (see Table II) $\delta A_{HOPG\text{-}clust} = 0.7$ eV, $\delta A_{HOPG\text{-}C_{60}} = 0.8$ eV, and $\delta A_{HOPG\text{-}\mathrm{SiC}} = -1.2$ eV. The Auger parameter in our film (552.9 eV) is far from that observed in 2H-SiC (554.8 eV) and differs slightly (0.7 eV) from that observed in HOPG (553.6 eV). The δA difference between the Si_xC_{1-x} film and the C_{60} film is negligible. This suggests that carbon in heterofullerenes presents all the features observed in C_{60} while silicon plays a minor role and does not affect significantly the host matrix.

Now, let us examine the oxidation process. ΔA increases strongly ($\Delta A = 1.5$ eV, 3.1 eV, and 6.1 eV for samples labeled I, II, and III, respectively). This indicates a decrease of the screening and a large chemical shift as observed in silicon oxides. The screening collapse is clearly emphasized by Eq. (11) since the dielectric constant in SiO_2 ($\epsilon_{0(\mathrm{SiO_2})} = 2.7$) is lower than in SiC ($\epsilon_{0(\mathrm{SiC})} = 6.7$). In the Penn model, it holds

$$\epsilon_0 = 1 + (\hbar\omega_p^2 / E_g) \tag{12}$$

holds, where ω_p and E_g are the plasma frequency and the Penn gap, respectively. Since the plasma frequency does not vary significantly, the Penn gap increases with the oxidation. It is well known that the Penn gap increases with the charge transfer,[47] for example, if the sole electron (i.e., the dangling bond) makes up a bonding with oxygen.

VII. CONCLUSION

Nonstoichiometric $Si_{0.12}C_{0.88}$ films elaborated by Si_qC_{2n-q} heterofullerene deposition exhibit electronic properties different from those observed in the SiC bulk phase. This SiC bonding is less stable than tetrahedral sp^3 bonding in the bulk phase. All the observed features can be modeled assuming a silicon atom surrounded by three carbon atoms. The sole electron plays the role of a dangling bond and can be easily bound to oxygen. Such behavior is in agreement with the structure predicted for the heterofullerenes. This type of bond might be observed by the extended x-ray-absorption fine structure (EXAFS) method performed on Si *K* edge. The correlation between local structural information and electronic structure will be discussed in a forthcoming paper. Besides, such heterofullerenes seem to be promising for building new materials. The so-called rehybridization, which characterizes the heterofullerenes, modifies the nature of the dangling bonds. The electron-spin-resonance method would be a powerful technique for this purpose.

ACKNOWLEDGMENTS

We wish to acknowledge Dr. B. Masenelli for helpful discussions.

[1] *Novel Refractory Semiconductors*, edited by D. Emin, T.L. Aselage, and C. Woods, Mater. Res. Soc. Symp. Proc. No. **97** (MRS, Pittsburgh, 1987).
[2] D.A. Anderson and W.E. Spear, Philos. Mag. **35**, 1 (1976).
[3] J. Huran, L. Hrubcin, A.P. Kobzev, and J. Liday, Vacuum **47**, 1223 (1996).
[4] A. Chehaidar, R. Carles, A. Zwick, C. Meunier, B. Cros, and J. Durand, J. Non-Cryst. Solids **169**, 37 (1994).
[5] K. Mui, and F.W. Smith, Phys. Rev. B **35**, 8080 (1986).
[6] F. Finocchi, G. Galli, M. Parinello, and C.M. Bartoni, Phys. Rev. Lett. **68**, 3044 (1992).
[7] P.C. Kelires, Phys. Rev. B **46**, 10 048 (1992).
[8] P. Mélinon, P. Kéghélian, A. Perez, C. Ray, J. Lermé, M. Pellarin, M. Broyer, M. Boudeulle, B. Champagnon, and J.L. Rousset, Phys. Rev. B **58**, 16 481 (1998).
[9] H.W. Kroto, J.R. Heath, S.C. O'Brien, R.F. Curl, and R.E. Smalley, Nature (London) **318**, 162 (1985).
[10] U. Röthlisberger, W. Andreoni, and M. Parinello, Phys. Rev. Lett. **72**, 665 (1994).
[11] E. Kaxiras, Phys. Rev. Lett. **64**, 551 (1990).
[12] M.V. Ramakrishna, and J. Pan, J. Chem. Phys. **101**, 8108 (1994).
[13] M.F. Jarrold and J.E. Bower, J. Chem. Phys. **96**, 9180 (1992).
[14] J.M. Alford, R.T. Laaksonen, and R.E. Smalley, J. Chem. Phys. **94**, 2618 (1990).
[15] P. Mélinon, P. Kéghélian, B. Prével, A. Perez, G. Guiraud, J. LeBrusq, J. Lermé, M. Pellarin, and M. Broyer, J. Chem. Phys. **107**, 10 278 (1997).
[16] J.L. Fye and M.F. Jarrold, J. Phys. Chem. A **101**, 1836 (1997).
[17] T. Kimura, T. Sugai, and H. Shinohara, Chem. Phys. Lett. **256**, 269 (1996).
[18] W. Branz, I.M.L. Billas, N. Malinowski, F. Tast, M. Heinebrodt, and T.P. Martin, J. Chem. Phys. **109**, 3425 (1998).
[19] C. Ray, M. Pellarin, J. Lermé, J.L. Vialle, M. Broyer, X. Blase, P. Mélinon, P. Kéghélian, and A. Perez, Phys. Rev. Lett. **80**, 5365 (1998).
[20] M. Pellarin, C. Ray, J. Lermé, J.L. Vialle, M. Broyer, X. Blase, P. Kéghélian, P. Mélinon, and A. Perez, J. Chem. Phys. **110**, 6927 (1999).

[21] In addition to mass-spectrometric measurements, photofragmentation experiments on selected clusters sizes have been carried out. Size distribution and photofragmentation provide evidence of the presence of heterofullerenes in the beam. The complete procedure is given in Ref. 20.

[22] This amorphous state could be explained by the spread in sizes and stoichiometry x (Si_xC_{1-x}) in the preformed clusters associated with the random distribution of the clusters on the substrate. In addition, the films appear nanogranular with a large void component between the deposited clusters. This involves a low film density associated with a large number of dangling bonds. However, the structure differs strongly from those observed in a-Si_xC_{1-x}:H compounds, where the homogeneity of the random distribution is much more. (P. Mélinon *et al.*, Philos. Mag. A **80**, 143 (2000).

[23] M. Balooch, R.J. Tench, W.J. Siekhaus, M.J. Allen, A.L. Connor, and D.R. Olander, Appl. Phys. Lett. **57**, 1540 (1990).

[24] The silver core-level line position remains constant before and after deposition. A depth profile obtained by ion etching does not reveal a significant shift due to silver-silicon or silver-carbon bonding.

[25] Most of the reference samples must be cleaved and prepared in UHV conditions. Since our samples are prepared *ex situ*, a low contamination with oxygen and hydrocarbon compounds is observed. This contamination could affect the AES/XPS features (broadening, fine structure, etc.). In fact, we assume that the position of the main lines is not affected and the Auger parameter remains valid. The contamination of the samples can be reduced by argon-ion etching. However, etching involves an amorphization that strongly affects the electronic structure, in particular, for carbon.

[26] P. Mélinon, P. Kéghélian, B. Prével, V. Dupuis, A. Perez, B. Champagnon, Y. Guyot, M. Pellarin, J. Lermé, M. Broyer, J.L. Rousset, and P. Delichére, J. Chem. Phys. **108**, 4607 (1998).

[27] Clusters are produced in a helium flux (99.9999% purity) without hydrogen. In an earlier work we checked by Fourier-transform infrared spectroscopy that Si-H or C-H modes gave a weak signal (Ref. 15).

[28] Previous measurements show that the stoichiometry in the film is correlated to the rod one. These assumptions are corroborated by Rutherford backscattering and energy dispersive x-ray spectroscopies performed on several systems [J.L. Rousset *et al.*, J. Phys. Chem. B **104**, 5430 (2000)].

[29] See *Diamond and Diamond-like Films and Coatings*, Vol. 266 of *NATO Advanced Studies Institute, Series B: Physics*, edited by R. E. Clausing, L. L. Horton, J. C. Angus, and P. Koidl (Plenum Press, New York, 1991).

[30] T. Takeshita, Y. Kurata, and S. Hasegawa, J. Appl. Phys. **71**, 5395 (1992).

[31] R.C. Fang and L. Ley, Phys. Rev. B **40**, 3818 (1989).

[32] The film is obtained by the deposition of C_{60} clusters. For this purpose the rod is constituted by sintered C_{60} powder.

[33] V. Paillard, P. Mlinon, V. Dupuis, J.P. Perez, and A. Perez, Phys. Rev. Lett. **71**, 4170 (1993).

[34] F. Ibrahim, J.I.B. Wilson, and P. John, J. Non-Cryst. Solids **91**, 200 (1995).

[35] P. Zhou, Z.H. Dong, A.M. Rao, and P.C. Eklund, Chem. Phys. Lett. **211**, 337 (1993).

[36] Y. Shi, X.J. Fan, H.X. Guo, and Q. Fu, Solid State Commun. **99**, 445 (1999).

[37] M. Hofmann, A. Zywietz, K. Karch, and F. Bechstedt, Phys. Rev. B **50**, 13 401 (1994).

[38] S. Kim, J.E. Spanier, and I.P. Herman, Jpn. J. Appl. Phys., Part 1 **39**, 5875 (2000).

[39] F. Bechstedt and R. Enderlein, Phys. Status Solidi B **94**, 239 (1979).

[40] F. Bechstedt, Phys. Status Solidi B **112**, 9 (1982).

[41] F. Bechstedt and K. Hübner, Phys. Status Solidi A **67**, 517 (1981).

[42] F. Bechstedt, Phys. Status Solidi B **91**, 167 (1979).

[43] Y.N. Xu, M.Z. Huang, and W.Y. Ching, Phys. Rev. B **46**, 4241 (1992).

[44] N.W. Ashcroft and N.D. Mermin, *Solid State Physics* (Saunders, Philadelphia, 1976).

[45] S.D. Waddington, in *Practical Surface Analysis*, edited by D. Briggs and M.P. Seah (Wiley, New York, 1990), Vol. 1, pp. 587–606.

[46] The Auger parameter is defined from the study of both Auger and photoelectron lines together in an XPS measurement. In our case, we use XPS and electron energy loss spectroscopy together. Moreover, the position of the Auger line is defined from the derivative signal rather than the Auger signal itself . Owing to this specific procedure, the Auger parameter does not coincide with usual value.

[47] O. Madelung, in *Introduction to Solid-State Theory*, edited by M. Cardona, P. Fulde, and H-J. Queisser, Solid-State Sciences, Vol. 2 (Springer-Verlag, Berlin, 1981), p. 347.